Int. J. Contemp. Math. Sciences, Vol. 4, 2009, no. 23, 1121 - 1147

Numerical Conformal Mapping of Bounded Multiply Connected Regions by an Integral Equation Method

Ali H. M. Murid and Laey-Nee Hu

Department of Mathematics, Faculty of Science
Universiti Teknologi Malaysia, 81310 UTM Skudai, Johor, Malaysia
ahmm@mel.fs.utm.my, huln1234@yahoo.com.my

Abstract

Conformal mappings are familiar tools in science and engineering. However exact mapping functions are unknown except for some special regions. In this paper, a boundary integral equation for conformal mapping $w = f(z)$ of multiply connected regions onto an annulus $\mu_1 < |w| < 1$ with circular slits $\mu_2, \mu_3, ..., \mu_M$ is presented. Our theoretical development is based on the boundary integral equation for conformal mapping of doubly connected region derived by Murid and Razali [12]. The boundary integral equation involved the unknown circular radii. For numerical experiments, the boundary integral equation with some normalizing conditions are discretized which leads to a system of nonlinear equations. This system is solved simultaneously using modification of the Gauss-Newton named Lavenberg-Marquardt with the Fletcher's algorithm for solving the nonlinear least squares problems. Once the boundary values of the mapping function are calculated, we can use the Cauchy's integral formula to determine the mapping function in the interior of the region. Numerical implementations on some test regions are also presented.

Mathematics Subject Classification: 30C30; 65R20; 65E05; 30C40; 45H15

Keywords: Conformal mapping, Integral equations, multiply connected regions, Neumann kernel, Lavenberg-Marquardt algorithm, Cauchy's integral formula

1 Introduction

Integral equation methods for conformal mapping of multiply connected regions is presently still a subject of interest. Nehari [13, p. 335] described the five types of slit region as important canonical regions for conformal mapping of multiply connected regions. They are the discs with concentric circular slits, an annulus with concentric circular slits, the circular slit region, the radial slit region and the parallel slit region. In general the radii of the circular slits are unknown and have to be determined in the course of the numerical evaluation. However, exact mapping functions are not known except for some special regions. In this paper we describe an integral equation method for computing the conformal mapping of multiply connected regions onto an annulus with concentric circular slits.

Several methods have been proposed in the literature for the numerical approximation for conformal mapping of multiply connected regions [1, 3, 5, 6, 8, 11, 12, 14, 15, 18]. One of the methods is the integral equation method. Some notable ones are the integral equations of Warschawski, Gerschgorin, and Symm. All these integral equations are extensions of those maps for simply connected regions. Recently, conformal mapping of doubly connected regions onto an annulus via the Kerzman-Stein and Neumann kernels are also discussed in Murid and Mohamed [11], and Mohamed [10, p. 51-88]. But Murid and Razali [12] and Mohamed [10] have not yet formulated an integral equation method based on the Neumann kernel for conformal mapping of bounded multiply connected regions onto an annulus with circular slits.

The plan of the paper is as follows : In Section 2, we derive a boundary integral equation satisfied by a function analytic on a multiply connected regions subjected to certain conditions. This derivation improves the boundary integral equation derived by Murid and Razali [12] which was limited to doubly connected regions. Furthermore it leads to a much simpler derivation of a system of an integral equations developed by Mohamed [10]. Another special case of this result is the integral equation involving the Neumann kernel related to conformal mapping of multiply connected regions onto an annulus with circular slits. In Section 3, we give an application of the theoretical result in Section 2 to conformal mapping of multiply connected regions. The numerical implementation for computing the mapping function is discussed in Section 4. Section 5 presents six numerical results as well as comparisons with the results of Amano [1], Murid and Mohamed [11], Mohamed [10], Symm [18], Reichel [15], Kokkinos *et al.* [8], Ellacott [5] and Okano *et al.* [14]. In Section 6 we draw some conclusions.

2 An Integral Equation Related to a Boundary Relationship

Let Γ_0, Γ_1, ..., Γ_M be $M+1$ smooth Jordan curves in the complex z-plane such that Γ_1, Γ_2, ..., Γ_M lies in the interior of Γ_0. Denote by Ω the bounded $(M+1)$-connected region bounded by Γ_0, Γ_1, ..., Γ_M. The positive direction of the contour $\Gamma = \Gamma_0 \cup \Gamma_1 \cup \cdots \cup \Gamma_M$ is usually that for which Ω is on the left as one traces the boundary (see Figure 1).

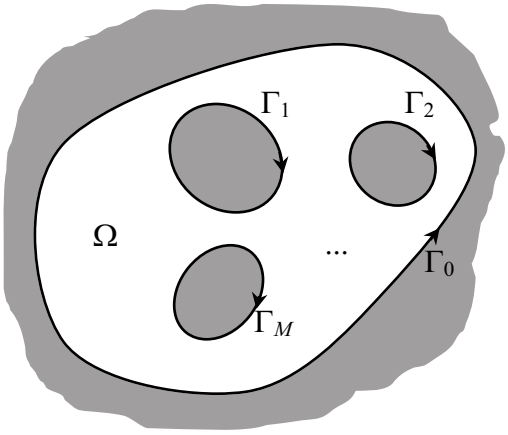

Figure 1: $(M+1)$-connected region Ω.

It is well known that if h is analytic and single-valued in Ω and continuous on $\Omega \cup \Gamma$, we have [7, p. 176]

$$\frac{1}{2\pi \mathrm{i}} \int_\Gamma \frac{h(w)}{w-z} dw = \frac{1}{2} h(z), \quad z \in \Gamma. \tag{1}$$

Suppose $D(z)$ is analytic and single-valued with respect to $z \in \Omega$ and is continuous on $\Omega \cup \Gamma$. Suppose further that D satisfies the boundary relationship

$$D(z) = c(z) \left[\frac{T(z) Q(z) D(z)}{P(z)} \right]^-, \quad z \in \Gamma, \tag{2}$$

where the minus sign in the superscript denotes complex conjugate, $T(z) = z'(t)/|z'(t)|$ is the complex unit tangent function at $z \in \Gamma$, while c, P, and Q are complex-valued functions defined on Γ with the following properties:

(P1) $P(z)$ is analytic and single-valued with respect to $z \in \Omega$,
(P2) $P(z)$ is continuous on $\Omega \cup \Gamma$,
(P3) $P(z)$ has a finite number of zeroes at $a_1, a_2, ..., a_M$ in Ω,
(P4) $c(z) \neq 0, P(z) \neq 0, Q(z) \neq 0, D(z) \neq 0, z \in \Gamma$.

Note that the boundary relationship (2) also has the following equivalent form:

$$P(z) = \overline{c(z)}\frac{T(z)Q(z)D(z)^2}{|D(z)|^2}, \quad z \in \Gamma. \tag{3}$$

By means of (1), an integral equation for D may be constructed that is related to the boundary relationship (2) as shown below:

Theorem 2.1 *Let u and v be any complex-valued functions that are defined on Γ. Then*

$$\begin{aligned}\frac{1}{2}\left[v(z) + \frac{u(z)}{\overline{T(z)Q(z)}}\right] D(z) + \\ \mathrm{PV}\frac{1}{2\pi \mathrm{i}}\int_\Gamma \left[\frac{c(z)u(z)}{c(w)(\overline{w}-\overline{z})\overline{Q(w)}} - \frac{v(z)T(w)}{w-z}\right] D(w)|dw| \\ = -c(z)u(z)\left[\sum_{a_j inside \Gamma} \operatorname*{Res}_{w=a_j} \frac{D(w)}{(w-z)P(w)}\right]^-, \quad z \in \Gamma,\end{aligned} \tag{4}$$

where the minus sign in the superscript denotes complex conjugation.

Proof. Consider the integral

$$I_1(z) = \mathrm{PV}\frac{1}{2\pi \mathrm{i}}\int_\Gamma \frac{v(z)T(w)D(w)}{w-z}|dw|, \quad z \in \Gamma. \tag{5}$$

Using $T(w)|d(w)| = dw$ and (1), since D is analytic on Ω, we obtain

$$I_1(z) = \frac{1}{2}v(z)D(z), \qquad z \in \Gamma. \tag{6}$$

Next we consider the integral

$$I_2(z) = \mathrm{PV}\frac{1}{2\pi \mathrm{i}}\int_\Gamma \frac{c(z)u(z)D(w)}{c(w)(\overline{w}-\overline{z})\overline{Q(w)}}|dw|, \quad z \in \Gamma. \tag{7}$$

Using the boundary relationship (3), $|D(w)|^2 = D(w)\overline{D(w)}$ and $\overline{T(w)}|dw| = \overline{dw}$, we get

$$I_2(z) = -c(z)u(z)\left[\frac{1}{2\pi \mathrm{i}}\int_\Gamma \frac{D(w)}{(w-z)P(w)}dw\right]^-. \tag{8}$$

Applying the residue theory and formula (1) to the integral in (8), $I_2(z)$ becomes

$$I_2(z) = -c(z)u(z)\left[\frac{1}{2}\frac{D(z)}{P(z)} + \sum_{a_j inside \Gamma} \operatorname*{Res}_{w=a_j} \frac{D(w)}{(w-z)P(w)}\right]^-. \tag{9}$$

Applying the boundary relationship (2) to the first term on the right-hand side yields

$$I_2(z) = -\frac{u(z)D(z)}{2\overline{T(z)Q(z)}} - c(z)u(z)\left[\sum_{a_j inside\Gamma} \operatorname*{Res}_{w=a_j} \frac{D(w)}{(w-z)P(w)}\right]^{-}. \tag{10}$$

Finally looking at $I_2(z) - I_1(z)$, yields

$$\begin{aligned} &\mathrm{PV}\frac{1}{2\pi \mathrm{i}} \int_\Gamma \frac{c(z)u(z)D(w)}{c(w)(\overline{w}-\overline{z})\overline{Q(w)}}|dw| - \mathrm{PV}\frac{1}{2\pi \mathrm{i}} \int_\Gamma \frac{v(z)T(w)D(w)}{(w-z)}|dw| \\ &\quad = -\frac{u(z)D(z)}{2\overline{T(z)Q(z)}} - c(z)u(z)\left[\sum_{a_j inside\Gamma} \operatorname*{Res}_{w=a_j} \frac{D(w)}{(w-z)P(w)}\right]^{-} \\ &\qquad - \frac{1}{2}v(z)D(z), \quad z \in \Gamma. \end{aligned} \tag{11}$$

Rearrangement of (11), gives (4). This completes the proof. ■

3 The Boundary Integral Equation for Conformal Mapping of Multiply Connected Regions

This section gives an application of Theorem 2.1 to conformal mapping of multiply connected regions. Let $w = f(z)$ be the analytic function which maps Ω conformally onto an annulus ($\mu_1 < |w| < \mu_0 = 1$) with circular slits of radii $\mu_2 < 1$, ..., $\mu_M < 1$ (see Figure 2). The mapping function f is determined up to a rotation of the annulus. The function f could be made unique by prescribing that

$$f'(a) > 0 \text{ or } f(z^*) = w^*,$$

where $a \in \Omega$, $z^* \in \Gamma_0$, and $w^* \in$ Unit Circle are fixed points.

The boundary value of f can be represented in form

$$f(z_0(t)) = e^{\mathrm{i}\theta_0(\mathrm{t})}, \quad \Gamma_0 : z = z_0(t), \quad 0 \le t \le \beta_0, \tag{12}$$

$$f(z_p(t)) = \mu_p e^{\mathrm{i}\theta_p(t)}, \Gamma_p : z = z_p(t), \quad 0 \le t \le \beta_p, \quad p = 1, 2, ..., M, \tag{13}$$

where $\theta_0(t), \theta_1(t), ..., \theta_M(t)$ are the boundary correspondence functions of Γ_0, Γ_1, ..., Γ_M respectively.

The unit tangent to Γ at $z(t)$ is denoted by $T(z(t)) = z'(t)/|z'(t)|$. Thus it can be shown that

$$f(z_0(t)) = \frac{1}{\mathrm{i}} T(z_0(t)) \frac{\theta_0'(t)}{|\theta_0'(t)|} \frac{f'(z_0(t))}{|f'(z_0(t))|} = \frac{1}{\mathrm{i}} T(z_0(t)) \frac{f'(z_0(t))}{|f'(z_0(t))|}, \quad z_0 \in \Gamma_0, \tag{14}$$

$$f(z_M(t)) = \frac{\mu_M}{\mathrm{i}} T(z_M(t)) \frac{\theta'_M(t)}{|\theta'_M(t)|} \frac{f'(z_M(t))}{|f'(z_M(t))|} = \frac{\mu_M}{\mathrm{i}} T(z_M(t)) \frac{f'(z_M(t))}{|f'(z_M(t))|}, \quad z_M \in \Gamma_M, \tag{15}$$

$$f(z_p(t)) = \frac{\mu_p}{\mathrm{i}} T(z_p(t)) \frac{\theta'_p(t)}{|\theta'_p(t)|} \frac{f'(z_p(t))}{|f'(z_p(t))|} = \pm \frac{\mu_p}{\mathrm{i}} T(z_p(t)) \frac{f'(z_p(t))}{|f'(z_p(t))|}, \quad z_p \in \Gamma_p. \tag{16}$$

for $p = 1, 2, ..., M-1$. Note that $\theta'_0(t) > 0$ and $\theta'_M(t) > 0$ while $\theta'_p(t)$ may be positive or negative since each circular slit $f(\Gamma_p)$ is traversed twice (see Figure 2). Thus $\theta'_p(t)/|\theta'_p(t)| = \pm 1$.

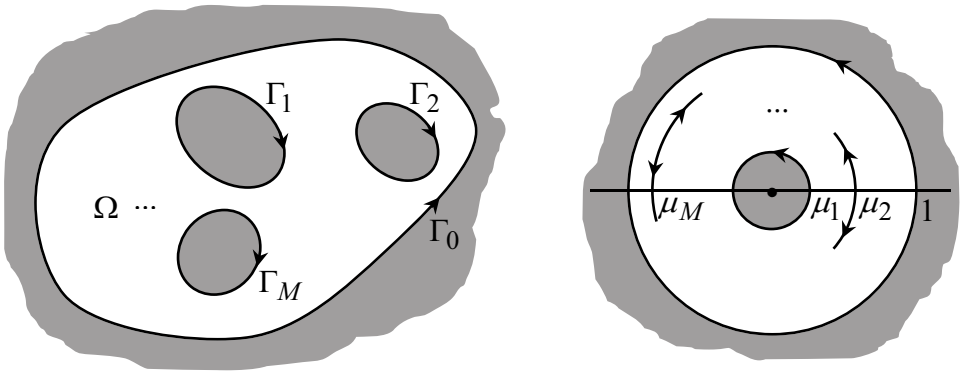

Figure 2: Mapping of a multiply connected region Ω.

The boundary relationships (14), (15) and (16) can be unified as

$$f(z) = \pm \frac{|f(z)|}{\mathrm{i}} T(z) \frac{f'(z)}{|f'(z)|}, \quad z \in \Gamma, \tag{17}$$

where $\Gamma = \Gamma_0 \cup \Gamma_1 \cup \cdots \cup \Gamma_M$. Note that the value of $|f(z)|$ is either 1, μ_M or μ_p for $z \in \Gamma$. However we cannot compare (17) with (3) due to the presence of the $\pm$ sign. To overcome this problem, we square both sides of the boundary relationship (17) to get

$$f(z)^2 = -|f(z)|^2 T(z)^2 \frac{f'(z)^2}{|f'(z)|^2}, \quad z \in \Gamma. \tag{18}$$

Comparison of (3) and (18) leads to a choice of $c(z) = -|f(z)|^2$, $P(z) = f(z)^2$, $D(z) = f'(z)$, $Q(z) = T(z)$, $u(z) = \overline{T(z)Q(z)}$ and $v(z) = 1$. Substituting these assignments into (4) leads to an integral equation satisfies by $f'(z)$, i.e.,

$$f'(z) + \mathrm{PV} \frac{1}{2\pi \mathrm{i}} \int_\Gamma \left[\frac{|f(z)|^2 \overline{T(z)^2}}{|f(w)|^2 (\overline{w} - \overline{z}) \overline{T(w)}} - \frac{T(w)}{(w - z)} \right] f'(w) |dw|$$

$$= |f(z)|^2\overline{T(z)^2}\left[\sum_{a_j inside\Gamma}\operatorname{Res}_{w=a_j}\frac{f'(w)}{(w-z)f(w)^2}\right]^{-}, \qquad z\in\Gamma. \quad (19)$$

For the case where Ω is a multiply connected regions being mapped onto an annulus with concentric circular slits, $f(z)$ does not have any zeroes in Ω. Thus the right-hand side of (19) vanishes and the integral equation (19) becomes

$$f'(z)+\mathrm{PV}\frac{1}{2\pi\mathrm{i}}\int_\Gamma\left[\frac{|f(z)|^2\overline{T(z)^2}}{|f(w)|^2(\overline{w}-\overline{z})\overline{T(w)}}-\frac{T(w)}{(w-z)}\right]f'(w)|dw|=0, \quad z\in\Gamma. \quad (20)$$

Multiply both sides by $T(z)$ and using the fact $T(z)\overline{T(z)}=|T(z)|^2=1$ gives

$$T(z)f'(z)+\mathrm{PV}\frac{1}{2\pi\mathrm{i}}\int_\Gamma\left[\frac{|f(z)|^2\overline{T(z)}}{|f(w)|^2(\overline{w}-\overline{z})}-\frac{T(z)}{(w-z)}\right]T(w)f'(w)|dw|=0, \quad z\in\Gamma. \quad (21)$$

The integral equation (21) can also be written briefly as

$$g(z)+\int_\Gamma N^*(z,w)g(w)|dw|=0, \qquad z\in\Gamma, \quad (22)$$

where

$$\begin{aligned} g(z) &= T(z)f'(z), \\ N^*(z,w) &= \frac{1}{2\pi\mathrm{i}}\left[\frac{T(z)}{(z-w)}-\frac{|f(z)|^2\overline{T(z)}}{|f(w)|^2(\overline{z}-\overline{w})}\right]. \end{aligned}$$

3.1 Conformal Mapping of Doubly Connected Regions

For the special case where Ω is a doubly connected region, the single integral equation in (22) can be separated into a system of equations

$$g(z_0)+\int_{\Gamma_0}N(z_0,w)g(w)|dw|-\int_{-\Gamma_1}P_0(z_0,w)g(w)|dw|=0, \quad z_0\in\Gamma_0, \quad (23)$$

$$g(z_1)+\int_{\Gamma_0}P_1(z_1,w)g(w)|dw|-\int_{-\Gamma_1}N(z_1,w)g(w)|dw|=0. \quad z_1\in\Gamma_1, \quad (24)$$

where

$$P_0(z,w) = \frac{1}{2\pi\mathrm{i}}\left[\frac{T(z)}{(z-w)}-\frac{\overline{T(z)}}{\mu_1^2(\overline{z}-\overline{w})}\right],$$

$$P_1(z,w) = \frac{1}{2\pi \mathrm{i}}\left[\frac{T(z)}{(z-w)} - \frac{\mu_1^2\overline{T(z)}}{(\overline{z}-\overline{w})}\right],$$

$$N(z,w) = \begin{cases} \dfrac{1}{2\pi \mathrm{i}}\left[\dfrac{T(z)}{z-w} - \dfrac{\overline{T(z)}}{\overline{z}-\overline{w}}\right], & \text{if } w, z \in \Gamma, w \neq z, \\ \dfrac{1}{2\pi}\dfrac{\mathrm{Im}[z''(t)\overline{z'(t)}]}{|z'(t)|^3}, & \text{if } w = z \in \Gamma. \end{cases}$$

The kernel N is also known as Neumann kernel. Note that the PV symbols are no longer required in (23) and (24) since the integrands are continuous along their respective paths of integrations. The integral equations (23) and (24) also involve the unknown parameter μ_1. Our derivations of this system of integral equation are much easier than the derivations given in Mohamed [10, p. 71-76]. Naturally it is also required that the unknown mapping function $f(z)$ be single-valued in the problem domain [6, p. 217], i.e.,

$$\int_{-\Gamma_1} f'(w)dw = 0 \tag{25}$$

which implies

$$\int_{-\Gamma_1} g(w)|dw| = 0. \tag{26}$$

Note that the system of integral equations consisting of (23), (24) and (26) is homogeneous and does not have a unique solution. To obtain a unique solution, we need to impose some conditions on $g(z)$. First, we consider applying the condition $f(z_0(0)) = 1$. From (14), this implies $g(z_0(0))/|g(z_0(0))| = \mathrm{i}$, which means

$$\mathrm{Re}\,[g(z_0(0))] = 0, \tag{27}$$

$$\mathrm{Im}\,[g(z_0(0))/|g(z_0(0)|] = 1. \tag{28}$$

Next we consider equation (12). Upon differentiation and taking modulus to both sides of equation (12), gives

$$|T(z_0(t))f'(z_0(t))z_0'(t)| = |T(z_0(t))e^{\mathrm{i}\theta_0(\mathrm{t})}\mathrm{i}\theta_0'(\mathrm{t})| = |\theta_0'(\mathrm{t})|. \tag{29}$$

Since the boundary correspondence function $\theta_0(t)$ is an increasing monotone function it's derivative is positive which implies $|\theta_0'(t)| = \theta_0'(t)$. Upon integrating (29) with respect to t form 0 to 2π gives

$$\int_0^{2\pi} |g(z_0(t))z_0'(t)|dt = \int_0^{2\pi} \theta_0'(t)dt = \theta_0(t)|_0^{2\pi} = 2\pi. \tag{30}$$

By the same reasoning, it can be shown that

$$\int_0^{2\pi} |g(z_1(t))z_1'(t)|dt = 2\pi\mu_1. \tag{31}$$

We note that, Mohamed [10, p. 75-82] however did not use the conditions (26), (27), (28), (30) and (31) to achieve uniqueness, but instead

$$\mu_1 \int_0^{2\pi} |g(z_0(t))z_0'(t)|dt - \int_0^{2\pi} |g(z_1(t))z_1'(t)|dt = 0$$

and

$$f'(z^*) = B^*$$

where B^* is predetermined.

Thus the system of integral equations comprising of (23), (24), (26) with the conditions (27), (28), (30) and (31) has a unique solution.

3.2 Conformal Mapping of Triply Connected Regions

For the special case where Ω is a triply connected regions being mapped onto an annulus with a concentric circular slit, the single integral equation in (22) can be separated into a system of equations

$$\begin{aligned} g(z_0) + \int_{\Gamma_0} N(z_0, w)g(w)|dw| - \int_{-\Gamma_1} P_0(z_0, w)g(w)|dw| \\ - \int_{-\Gamma_2} Q_0(z_0, w)g(w)|dw| = 0, \quad z_0 \in \Gamma_0, \end{aligned} \tag{32}$$

$$\begin{aligned} g(z_1) + \int_{\Gamma_0} P_1(z_1, w)g(w)|dw| - \int_{-\Gamma_1} N(z_1, w)g(w)|dw| \\ - \int_{-\Gamma_2} Q_1(z_1, w)g(w)|dw| = 0, \quad z_1 \in \Gamma_1, \end{aligned} \tag{33}$$

$$\begin{aligned} g(z_2) + \int_{\Gamma_0} P_2(z_2, w)g(w)|dw| - \int_{-\Gamma_1} Q_2(z_2, w)g(w)|dw| \\ - \int_{-\Gamma_2} N(z_2, w)g(w)|dw| = 0, \quad z_2 \in \Gamma_2, \end{aligned} \tag{34}$$

where

$$\begin{aligned} Q_0(z, w) &= \frac{1}{2\pi \mathrm{i}} \left[\frac{T(z)}{(z-w)} - \frac{\overline{T(z)}}{\mu_2^2(\overline{z} - \overline{w})} \right], \\ Q_1(z, w) &= \frac{1}{2\pi \mathrm{i}} \left[\frac{T(z)}{(z-w)} - \frac{\mu_1^2}{\mu_2^2} \frac{\overline{T(z)}}{(\overline{z} - \overline{w})} \right], \\ P_2(z, w) &= \frac{1}{2\pi \mathrm{i}} \left[\frac{T(z)}{(z-w)} - \frac{\mu_2^2 \overline{T(z)}}{(\overline{z} - \overline{w})} \right], \\ Q_2(z, w) &= \frac{1}{2\pi \mathrm{i}} \left[\frac{T(z)}{(z-w)} - \frac{\mu_2^2}{\mu_1^2} \frac{\overline{T(z)}}{(\overline{z} - \overline{w})} \right]. \end{aligned}$$

As in the doubly connected case, several additional conditions are required to help achieve uniqueness. The single-valuedness requirement on the mapping function $f(z)$ implies

$$\int_{-\Gamma_1} g(w)|dw| = 0, \quad \int_{-\Gamma_2} g(w)|dw| = 0. \tag{35}$$

The set of equation (32) to (35) does not guarantee a unique solution. The conditions (27), (28), (30) and (31) are also valid for the triply connected case under consideration. If the triply connected region is symmetric with respect to the axes, we can also impose the conditions

$$\mathrm{Re}\,[g(z_1(0))] = 0, \tag{36}$$

$$\mathrm{Re}\,[g(z_2(0))] = 0. \tag{37}$$

4 Numerical Implementation

In this section we first describe in detail a numerical method for computing the mapping function $f(z)$ and μ_1 for the case of a doubly connected region. Using the parametric representations $z_0(t)$ of Γ_0 for $t : 0 \le t \le \beta_0$ and $z_1(t)$ of $-\Gamma_1$ for $t : 0 \le t \le \beta_1$ the system of integral equation (23), (24), (26), (30) and (31) become

$$g(z_0(t)) + \int_0^{\beta_0} N(z_0(t), z_0(s))g(z_0(s))|z_0'(s)|ds - \int_0^{\beta_1} P(z_0(t), z_1(s))g(z_1(s))|z_1'(s)|ds = 0, \quad z_0(t) \in \Gamma_0, \tag{38}$$

$$g(z_1(t)) + \int_0^{\beta_0} Q(z_1(t), z_0(s))g(z_0(s))|z_0'(s)|ds - \int_0^{\beta_1} N(z_1(t), z_1(s))g(z_1(s))|z_1'(s)|ds = 0, \quad z_1(t) \in \Gamma_1, \tag{39}$$

$$\int_0^{\beta_1} g(z_1(s))|z_1'(s)|ds = 0, \tag{40}$$

$$\int_0^{\beta_0} |g(z_0(s))z_0'(s)|ds = 2\pi, \tag{41}$$

$$\int_0^{\beta_1} |g(z_1(s))z_1'(s)|ds = 2\pi\mu_1. \tag{42}$$

Multiply (38) and (39) respectively by $|z_0'(t)|$ and $|z_1'(t)|$ gives

$$|z_0'(t)|g(z_0(t)) + \int_0^{\beta_0} |z_0'(t)|N(z_0(t), z_0(s))g(z_0(s))|z_0'(s)|ds$$

$$-\int_0^{\beta_1} |z_0'(t)|P(z_0(t),z_1(s))g(z_1(s))|z_1'(s)|ds = 0, \quad z_0(t)\in\Gamma_0, \tag{43}$$

$$|z_1'(t)|g(z_1(t)) + \int_0^{\beta_0} |z_1'(t)|Q(z_1(t),z_0(s))g(z_0(s))|z_0'(s)|ds$$
$$-\int_0^{\beta_1} |z_1'(t)|N(z_1(t),z_1(s))g(z_1(s))|z_1'(s)|ds = 0, \quad z_1(t)\in\Gamma_1. \tag{44}$$

Defining

$$\begin{aligned}
\phi_0(t) &= |z_0'(t)|g(z_0(t)),\\
\phi_1(t) &= |z_1'(t)|g(z_1(t)),\\
K_{00}(t_0,s_0) &= |z_0'(t)|N(z_0(t),z_0(s)),\\
K_{01}(t_0,s_1) &= |z_0'(t)|P(z_0(t),z_1(s)),\\
K_{10}(t_1,s_0) &= |z_1'(t)|Q(z_1(t),z_0(s)),\\
K_{11}(t_1,s_1) &= |z_1'(t)|N(z_1(t),z_1(s)),
\end{aligned}$$

the system of equations (43), (44), (40), (41), (42), (27) and (28) can be briefly written as

$$\phi_0(t) + \int_0^{\beta_0} K_{00}(t_0,s_0)\phi_0(s)ds - \int_0^{\beta_1} K_{01}(t_0,s_1)\phi_1(s)ds = 0, \tag{45}$$

$$\phi_1(t) + \int_0^{\beta_0} K_{10}(t_1,s_0)\phi_0(s)ds - \int_0^{\beta_1} K_{11}(t_1,s_1)\phi_1(s)ds = 0, \tag{46}$$

$$\int_0^{\beta_1} \phi_1(s)ds = 0, \tag{47}$$

$$\int_0^{\beta_0} |\phi_0(s)|ds = 2\pi, \tag{48}$$

$$\int_0^{\beta_1} |\phi_1(s)|ds = 2\pi\mu_1, \tag{49}$$

$$\mathrm{Re}\,\phi_0(0) = 0, \tag{50}$$

$$\mathrm{Im}\,[\phi_0(0)/|\phi_0(0)|] = 1. \tag{51}$$

Since the functions ϕ and K in the above systems are β-periodic, a reliable procedure for solving (45) to (49) numerically is by using the Nyström's method [2] with the trapezoidal rule . The trapezoidal rule is the most accurate method for integrating periodic functions numerically [4, p. 134-142]. We choose $\beta_0 = \beta_1 = 2\pi$ and n equidistant collocation points $t_i = (i-1)\beta_0/n$, $1 \le i \le n$ on Γ_0 and m equidistant collocation points $t_{\tilde{i}} = (\tilde{i}-1)\beta_1/m$, $1 \le \tilde{i} \le m$, on Γ_1. Applying the Nyström's method with trapezoidal rule to discretize (45) to (49), we obtain

$$\phi_0(t_i) + \frac{\beta_0}{n}\sum_{j=1}^{n} K_{00}(t_i,t_j)\phi_0(t_j) - \frac{\beta_1}{m}\sum_{\tilde{j}=1}^{m} K_{01}(t_i,t_{\tilde{j}})\phi_1(t_{\tilde{j}}) = 0, \tag{52}$$

$$\phi_1(t_{\tilde{i}}) + \frac{\beta_0}{n}\sum_{j=1}^{n} K_{10}(t_{\tilde{i}}, t_j)\phi_0(t_j) - \frac{\beta_1}{m}\sum_{\tilde{j}=1}^{m} K_{11}(t_{\tilde{i}}, t_{\tilde{j}})\phi_1(t_{\tilde{j}}) = 0, \quad (53)$$

$$\sum_{\tilde{j}=1}^{m} \phi_1(t_{\tilde{j}}) = 0, \quad (54)$$

$$\sum_{j=1}^{n} |\phi_0(t_j)| = n, \quad (55)$$

$$\sum_{j=1}^{n} |\phi_1(t_j)| = n\mu_1. \quad (56)$$

Equations (52) to (56) lead to a system of $(n+m+3)$ non-linear complex equations in n unknowns $\phi_0(t_i)$, m unknowns $\phi_1(t_{\tilde{i}})$ and μ_1. By defining the matrices

$$\begin{aligned} B_{ij} &= \frac{\beta_0}{n}K_{00}(t_i, t_j), & C_{i\tilde{j}} &= \frac{\beta_1}{m}K_{01}(t_i, t_{\tilde{j}}), \\ D_{\tilde{i}j} &= \frac{\beta_0}{n}K_{10}(t_{\tilde{i}}, t_j), & E_{\tilde{i}\tilde{j}} &= \frac{\beta_1}{m}K_{11}(t_{\tilde{i}}, t_{\tilde{j}}), \\ x_{0i} &= \phi_0(t_i), & x_{1\tilde{i}} &= \phi_1(t_{\tilde{i}}), \end{aligned}$$

the system of equations (52) and (53) can be written as $n+m$ by $n+m$ system of equations

$$[I_{nn} + B_{nn}]\mathbf{x}_{0n} - C_{nm}\mathbf{x}_{1m} = 0, \quad (57)$$

$$D_{mn}\mathbf{x}_{0n} + [I_{mm} - E_{mm}]\mathbf{x}_{1m} = 0. \quad (58)$$

The result in matrix form for the system of equations (57) and (58) is

$$\begin{pmatrix} I_{nn} + B_{nn} & \cdots & -C_{nm} \\ \vdots & \cdots & \vdots \\ D_{mn} & \cdots & I_{mm} - E_{mm} \end{pmatrix} \begin{pmatrix} \mathbf{x}_{0n} \\ \vdots \\ \mathbf{x}_{1m} \end{pmatrix} = \begin{pmatrix} 0_{0n} \\ \vdots \\ 0_{1m} \end{pmatrix}. \quad (59)$$

Defining

$$\mathbf{A} = \begin{pmatrix} I_{nn} + B_{nn} & \cdots & -C_{nm} \\ \vdots & \cdots & \vdots \\ D_{mn} & \cdots & I_{mm} - E_{mm} \end{pmatrix}, \ \mathbf{x} = \begin{pmatrix} \mathbf{x}_{0n} \\ \vdots \\ \mathbf{x}_{1m} \end{pmatrix} \text{ and } \mathbf{0} = \begin{pmatrix} 0_{0n} \\ \vdots \\ 0_{1m} \end{pmatrix},$$

the $(n+m)\times(n+m)$ system can be written briefly as $\mathbf{Ax} = \mathbf{0}$. Separating $\mathbf{A}$ and $\mathbf{x}$ in terms of the real and imaginary parts, the system can be written as

$$\mathrm{Re}\,\mathbf{A}\,\mathrm{Re}\,\mathbf{x} - \mathrm{Im}\,\mathbf{A}\,\mathrm{Im}\,\mathbf{x} + \mathrm{i}(\,\mathrm{Im}\mathbf{A}\,\mathrm{Re}\,\mathbf{x} + \mathrm{Re}\,\mathbf{A}\,\mathrm{Im}\,\mathbf{x}) = \mathbf{0} + \mathbf{0}\mathrm{i}. \quad (60)$$

The single $(n+m)\times(n+m)$ complex system (60) above is equivalent to the $2(n+m)\times 2(n+m)$ system matrix involving the real (Re) and imaginary (Im) of the unknown functions, i.e.,

$$\begin{pmatrix} \mathrm{Re\ A} & \cdots & \mathrm{Im\ A} \\ \vdots & \cdots & \vdots \\ \mathrm{Im\ A} & \cdots & \mathrm{Re\ A} \end{pmatrix} \begin{pmatrix} \mathrm{Re}\,\mathbf{x} \\ \vdots \\ \mathrm{Im}\,\mathbf{x} \end{pmatrix} = \begin{pmatrix} 0 \\ \vdots \\ 0 \end{pmatrix}. \tag{61}$$

Note that the matrix in (61) contains the unknown parameter μ_1.
Since $\phi = \mathrm{Re}\,\phi + \mathrm{i}\,\mathrm{Im}\,\phi$, equations (54), (55), (56), (50) and (51) becomes

$$\sum_{\tilde{j}=1}^{m}(\mathrm{Re}\,x_{1\tilde{j}} + \mathrm{i}\,\mathrm{Im}\,x_{1\tilde{j}}) = 0, \tag{62}$$

$$\sum_{j=1}^{n}\sqrt{(\mathrm{Re}\,x_{0j})^2 + (\mathrm{Im}\,x_{0j})^2} = n, \tag{63}$$

$$\sum_{\tilde{j}=1}^{m}\sqrt{(\mathrm{Re}\,x_{1\tilde{j}})^2 + (\mathrm{Im}\,x_{1\tilde{j}})^2} = n\mu_1, \tag{64}$$

$$\mathrm{Re}\,x_{01} = 0, \tag{65}$$

$$\mathrm{Im}\,[x_{01}/\sqrt{(\mathrm{Re}\,x_{01})^2 + (\mathrm{Im}\,x_{01})^2}] = 1. \tag{66}$$

We next proceed to solve simultaneously the real nonlinear system in (61) with the equations (62) to (66) which also involves the Re and Im parts of the unknown functions. This system is an over-determined system of nonlinear equations involving $2(n+m)+5$ equations in $2(n+m)+1$ unknowns. Methods for solving over-determined system are best dealt with as problems in optimization [21, p. 146]. We use a modification of the Gauss-Newton called the Lavenberg-Marquardt with the Fletcher's algorithm [19, p. 233-246] to solve this nonlinear least square problem. Our nonlinear least square problem consists in finding the vector $\mathbf{x}$ for which the function $S : R^{2(n+m)+5} \to R^1$ defined by the sum of squares

$$S(\mathbf{x}) = \mathbf{f}^{\mathrm{T}}\mathbf{f} = \sum_{i=1}^{2(n+m)+5} (f_i(\mathbf{x}))^2$$

is minimal. Here, $\mathbf{x}$ stands for the $2(n+m)+1$ vector ($\mathrm{Re}\,x_{01}$, $\mathrm{Re}\,x_{02}$, ..., $\mathrm{Re}\,x_{0n}$, $\mathrm{Re}\,x_{11}$, $\mathrm{Re}\,x_{12}$, ..., $\mathrm{Re}\,x_{1m}$, $\mathrm{Im}\,x_{01}$, $\mathrm{Im}\,x_{02}$, ..., $\mathrm{Im}\,x_{0n}$, $\mathrm{Im}\,x_{11}$, $\mathrm{Im}\,x_{12}$, ..., $\mathrm{Im}\,x_{1m}$, μ_1), and $\mathbf{f} = (f_1, f_2, ..., f_{2(n+m)+5})$. The Lavenberg-Marquardt algorithm is an iterative procedure with starting value denoted as $\mathbf{x}_0$. This initial approximation, which, if at all possible, should be well-informed guess and generate a sequence of approximations $\mathbf{x}_1$, $\mathbf{x}_2$, $\mathbf{x}_3$, ... base on the formula

$$\mathbf{x}_{k+1} = \mathbf{x}_k - H(\mathbf{x}_k)\mathbf{f}(\mathbf{x}_k), \qquad \lambda_k \geq 0, \tag{67}$$

where $H(\mathbf{x}_k) = ((J_{\mathbf{f}}(\mathbf{x}_k))^T J_{\mathbf{f}}(\mathbf{x}_k) + \lambda_k I)^{-1}(J_{\mathbf{f}}(\mathbf{x}_k))^T$.
Our strategy for getting the initial estimation $\mathbf{x}_0$ is based on (12) and (13) which upon differentiating, we obtain

$$\begin{aligned}\phi_0(t) &= f'(z_0(t))z_0'(t) = \mathrm{i}\theta_0'(\mathrm{t})\mathrm{e}^{\mathrm{i}\theta_0(\mathrm{t})},\\ \phi_1(t) &= f'(z_1(t))z_1'(t) = \mu_1\mathrm{i}\theta_1'(\mathrm{t})\mathrm{e}^{\mathrm{i}\theta_1(\mathrm{t})}.\end{aligned}$$

For initial estimation, we assume $\theta_0(t) = \theta_1(t) = t$ which implies $\theta_0'(t) = \theta_1'(t) = 1$ and choose $\mu_1 = 0.5$ as our initial guess of the inner radius. In all our experiments, we have chosen the number of collocation points on Γ_0 and Γ_1 being equal, i.e., $n = m$. Having solved the system of equations for the unknown functions $\phi_0(t) = |z_0'(t)|T(z_0(t))f'(z_0(t))$, $\phi_1(t) = |z_1'(t)|T(z_1(t))f'(z_1(t))$ and μ_1, the boundary correspondence functions $\theta_0(t)$ and $\theta_1(t)$ are then computed approximately by the formulas

$$\begin{aligned}\theta_0(t) &= \mathrm{Arg}\, f(z_0(t)) \approx \mathrm{Arg}\,(-\mathrm{i}\phi_0(t)),\\ \theta_1(t) &= \mathrm{Arg}\, f(z_1(t)) \approx \mathrm{Arg}\,(-\mathrm{i}\phi_1(t)).\end{aligned}$$

We note that the numerical implementation described here are basically the same as in Mohamed [10] but with set of conditions different from (47) to (51).

Once the boundary values of the mapping function f are known, the values of the mapping function may be calculated by quadrature at any interior points of its domain of definition through Cauchy's integral formula for doubly connected region which read as follows:

Theorem 4.1 (Cauchy's Integral Formula) *Let f be analytic on the boundaries $\Gamma = \Gamma_0 \cup \Gamma_1$ and the region Ω bounded by Γ_0 and Γ_1. If ζ is any point on Ω, then*

$$\begin{aligned}f(\zeta) &= \frac{1}{2\pi\mathrm{i}}\int_{\Gamma}\frac{f(z)}{z-\zeta}dz\\ &= \frac{1}{2\pi\mathrm{i}}\int_{\Gamma_0}\frac{f(z)}{z-\zeta}dz - \frac{1}{2\pi\mathrm{i}}\int_{-\Gamma_1}\frac{f(z)}{z-\zeta}dz. \qquad (68)\end{aligned}$$

The Cauchy's integral formula (68) can be also written in the parametrized form, i.e.

$$f(\zeta) = \frac{1}{2\pi\mathrm{i}}\int_0^{\beta_0}\frac{f(z_0(t))z_0'(t)}{z_0(t)-\zeta}dt - \frac{1}{2\pi\mathrm{i}}\int_0^{\beta_1}\frac{f(z_1(t))z_1'(t)}{z_1(t)-\zeta}dt. \qquad (69)$$

By means of (12) and (13), the Cauchy's integral formula (68) can then be written in the form

$$f(\zeta) = \frac{1}{2\pi\mathrm{i}}\int_0^{\beta_0}\frac{e^{\mathrm{i}\theta_0(t)}z_0'(t)}{z_0(t)-\zeta}dt - \frac{1}{2\pi\mathrm{i}}\int_0^{\beta_1}\frac{\mu_1 e^{\mathrm{i}\theta_1(t)}z_1'(t)}{z_1(t)-\zeta}dt. \qquad (70)$$

For the points which are not close to the boundary, the integrands are well behaved. However for points near the boundary, the numerical integration is inaccurate due to the influence of the singularity. This difficulty is overcome through the introduction of an iterative technique as given in [17, p. 303]. If we define $f_0(\zeta)$ to be $f(z)$ where z is a point on the boundary which is closest to ζ, then we can define

$$f_{k+1}(\zeta) = \frac{1}{2\pi \mathrm{i}} \int_\Gamma \frac{f(z) - f_k(\zeta)}{z - \zeta} dz + f_k(\zeta). \tag{71}$$

In practice the iteration converges rapidly. Using this technique, we are able to maintain the same accuracy throughout the region Ω.

The numerical implementation for the case where Ω is a triply connected regions being mapped onto an annulus with concentric circular slit is similar with doubly connected regions.

5 Numerical Results

For numerical experiments, we have used some common test regions based on the examples given in [1, 5, 8, 10, 11, 15, 18]. All the computations are done using MATHEMATICA package [20] in single precision (16 digit machine precision).

5.1 Doubly Connected Regions

We have used four test regions whose exact boundary correspondence functions are known. The test regions are circular frame, frame of Limacon, elliptic frame and frame of Cassini's oval. N number of collocation points on each boundary has been chosen. The results for the sub-norm error between the exact values of $\theta_0(t)$, $\theta_1(t)$, μ_1 and their corresponding approximations $\theta_{0n}(t)$, $\theta_{1n}(t)$, μ_{1n} are shown in Tables 1, 5, 9 and 13. The numerical computations for these regions are compared with those obtained by Murid and Mohamed [11], and Mohamed [10] based on the Kerzman-Stein and Neumann kernels. We also compare our numerical results with those obtained by Amano [1] and Symm [18], though their distribution are different from ours. The notation E_M and E_A that are used by Amano and Symm are defined as follows:

$$\begin{aligned} E_M &= \max\{\max_i ||f(z_0(t_i))| - 1|, \max_i ||f(z_1(t_i))| - \mu_1|\}, \\ E_A &= \max\{\|\theta_0(t) - \theta_{0n}(t)\|_\infty, \|\theta_1(t) - \theta_{1n}(t)\|_\infty\}. \end{aligned}$$

Some integral equations do not involve the modulus μ_1^{-1} of the given doubly connected region such as the Warschawski's and Gershgorin's integral equations. In such cases, the functions $\theta_0(t)$, $\theta_1(t)$ are determined first. Then, the

modulus is computed from the following formula [6, p. 461-468]

$$\begin{aligned}\operatorname{Log}\frac{1}{\mu_1} &= \operatorname{Log}\left|\frac{z_0(0)-\omega}{z_1(0)-\omega}\right| - \frac{1}{2\pi}\int_0^{\beta_0}\operatorname{Re}\frac{z_0'(t)}{z_0(t)-\omega}\theta_0(t)dt \\ &\quad + \frac{1}{2\pi}\int_0^{\beta_1}\operatorname{Re}\frac{z_1'(t)}{z_1(t)-\omega}\theta_1(t)dt, \end{aligned} \tag{72}$$

for ω is a any arbitrary point z interior to Γ_1.

In this paper we have used our computed solutions $\theta_{0n}(t)$ and $\theta_{1n}(t)$ to approximate μ_1, represented by μ_{1n}^*, based on the formula (72). Since $\theta_{0n}(t)$ and $\theta_{1n}(t)$ are computed based on Nyström's method with trapezoidal rule, the approximation μ_{1n}^* is calculated by means of

$$\begin{aligned}\operatorname{Log}\frac{1}{\mu_{1n}^*} &= \operatorname{Log}\left|\frac{z_0(0)-\omega}{z_1(0)-\omega}\right| - \frac{1}{n}\sum_{i=1}^{n}\operatorname{Re}\frac{z_0'(t_i)}{z_0(t_i)-\omega}\theta_0(t_i) \\ &\quad + \frac{1}{n}\sum_{i=1}^{n}\operatorname{Re}\frac{z_1'(t_i)}{z_1(t_i)-\omega}\theta_1(t_i). \end{aligned} \tag{73}$$

The error norm $\|\mu_1 - \mu_{1n}^*\|$ are also displayed in the tables.

Example 5.1 *Frame of Cassini's Oval :*
If Ω is the region bounded by two Cassini's oval, then the complex parametric equation of its boundary is given by [1],

$$\begin{aligned}\Gamma_0 : \{z(t) &= \sqrt{b_0^2\cos 2t + \sqrt{a_0^4 - b_0^4\sin^2 2t}}\, e^{\mathrm{i}t}, a_0 > 0, b_0 > 0\}, \\ \Gamma_1 : \{z(t) &= \sqrt{b_1^2\cos 2t + \sqrt{a_1^4 - b_1^4\sin^2 2t}}\, e^{\mathrm{i}t}, a_1 > 0, b_1 > 0\}, \quad 0 \le t \le 2\pi. \end{aligned}$$

such that

$$\Omega : |z^2 - b_0^2| < a_0^2, \qquad |z^2 - b_1^2| > a_1^2,$$

The boundaries Γ_0 and Γ_1 are chosen such that $(a_0^4 - b_0^4)/b_0^2 = (a_1^4 - b_1^4)/b_1^2$. Then the exact mapping function is given by

$$f(z) = \frac{a_0 z}{\sqrt{b_0^2 z^2 + a_0^4 - b_0^4}}, \quad \mu_1 = \frac{a_0 b_1}{a_1 b_0}.$$

Figure 3 shows the region and image based on our method. Tables 1, 2, 3 and 4 show our results together with the results of Murid and Mohamed [11], Mohamed [10], Amano [1] and Symm [18].

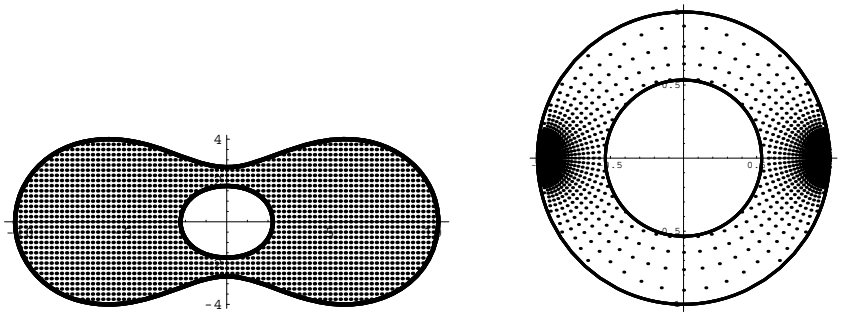

Figure 3: Frame of Cassini's Oval : a rectangular grid in Ω with grid size 0.25 and its image with $a_0 = 2\sqrt{14}, a_1 = 2, b_0 = 7$, and $b_1 = 1$.

Table 1: Error Norm (Frame of Cassini's oval) using our method

N	$\|\theta_0(t) - \theta_{0n}(t)\|_\infty$	$\|\theta_1(t) - \theta_{1n}(t)\|_\infty$	$\|\mu_1 - \mu_{1n}\|_\infty$	$\|\mu_1 - \mu^*_{1n}\|_\infty$
16	6.3(−03)	1.9(−03)	1.5(−03)	3.7(−03)
32	6.0(−05)	1.6(−05)	1.3(−05)	2.0(−03)
64	3.2(−08)	1.2(−08)	1.8(−09)	5.4(−04)
128	1.9(−08)	7.1(−09)	0	1.3(−04)

Table 2: Error Norm (Frame of Cassini's oval) as given in [10] based on the Neumann kernel

N	$\|\theta_0(t) - \theta_{0n}(t)\|_\infty$	$\|\theta_1(t) - \theta_{1n}(t)\|_\infty$	$\|\mu_1 - \mu_{1n}\|_\infty$
16	6.4(−03)	1.9(−03)	1.5(−03)
32		does not converge	
64	3.1(−02)	1.9(−02)	8.9(−07)

Table 3: Error Norm (Frame of Cassini's oval) as given in [10, 11] based on the Kerzman-Stein kernel

N	$\|\theta_0(t) - \theta_{0n}(t)\|_\infty$	$\|\theta_1(t) - \theta_{1n}(t)\|_\infty$	$\|\mu_1 - \mu_{1n}\|_\infty$
16	6.4(−03)	2.5(−03)	2.1(−03)
32	6.9(−05)	2.7(−05)	2.1(−05)
64	1.1(−08)	3.7(−09)	3.9(−09)

Example 5.2 *Elliptic Frame :*
Elliptic frame is the domain bounded by two Jordan curves, Γ_0 and Γ_1 such

Table 4: Error Norm (Frame of Cassini's oval) using Amano's method and Symm's method

Amano's Method			Symm's Method	
N	E_M	E_A	N	E_M
16	9.1(−03)	9.7(−03)	64	1.94(−02)
32	3.4(−04)	3.8(−04)	128	3.00(−03)
64	6.9(−07)	5.0(−08)	256	7.00(−04)
128	7.7(−11)	7.7(−11)		

that

$$\Omega : \frac{x^2}{a_0^2} + \frac{y^2}{b_0^2} < 1, \qquad \frac{x^2}{a_1^2} + \frac{y^2}{b_1^2} > 1,$$

with the complex parametric of its boundary is given by [1]

$$\begin{aligned} \Gamma_0 : \{z(t) &= a_0 \cos t + \mathrm{i} b_0 \sin t, a_0 > 0, b_0 > 0\}, \\ \Gamma_1 : \{z(t) &= a_1 \cos t + \mathrm{i} b_1 \sin t, a_1 > 0, b_1 > 0\}, \quad 0 \le t \le 2\pi. \end{aligned}$$

When the two ellipses Γ_0 and Γ_1 are confocal such that $a_0^2 - b_0^2 = a_1^2 - b_1^2$, the exact mapping function is given by

$$f(z) = \frac{z + \sqrt{z^2 - (a_0^2 - b_0^2)}}{a_0 + b_0}, \quad \mu_1 = \frac{a_1 + b_1}{a_0 + b_0}.$$

Figure 4 shows the region and image based on our method. Tables 5, 6, 7 and 8 show our results together with the results of Murid and Mohamed [11], Mohamed [10], Amano [1] and Symm [18].

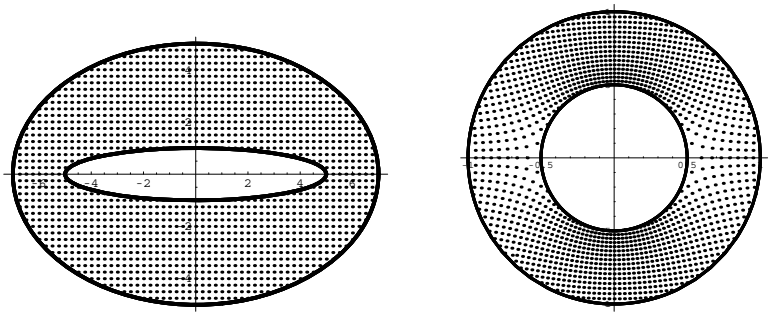

Figure 4: Elliptic Frame : a rectangular grid in Ω with grid size 0.25 and its image with $a_0 = 7, a_1 = 5, b_0 = 5$ and $b_1 = 1$.

Table 5: Error Norm (Elliptic Frame) using our method

N	$\|\theta_0(t) - \theta_{0n}(t)\|_\infty$	$\|\theta_1(t) - \theta_{1n}(t)\|_\infty$	$\|\mu_1 - \mu_{1n}\|_\infty$	$\|\mu_1 - \mu^*_{1n}\|_\infty$
16	2.3(−03)	6.6(−03)	2.0(−04)	9.4(−03)
32	3.5(−06)	9.9(−06)	3.6(−06)	1.1(−03)
64	1.9(−08)	1.7(−08)	7.0(−12)	1.9(−04)
128	7.6(−09)	6.7(−09)	5.6(−17)	4.7(−05)

Table 6: Error Norm (Elliptic frame) as given in [10] based on the Neumann kernel

N	$\|\theta_0(t) - \theta_{0n}(t)\|_\infty$	$\|\theta_1(t) - \theta_{1n}(t)\|_\infty$	$\|\mu_1 - \mu_{1n}\|_\infty$
16	1.1	3.1	7.2(−02)
32	2.3(−05)	2.4(−05)	3.0(−06)
64	1.3(−07)	1.5(−07)	7.0(−12)

Table 7: Error Norm (Elliptic frame) as given in [10, 11] based on the Kerzman-Stein kernel

N	$\|\theta_0(t) - \theta_{0n}(t)\|_\infty$	$\|\theta_1(t) - \theta_{1n}(t)\|_\infty$	$\|\mu_1 - \mu_{1n}\|_\infty$
16	4.0(−04)	3.2(−04)	3.7(−05)
32	5.1(−06)	1.0(−05)	3.7(−06)
64	2.7(−09)	5.9(−09)	2.2(−09)
128	3.6(−15)	5.8(−15)	1.8(−15)

Table 8: Error norm (Elliptic frame) using Amano's method and Symm's method

Amano's Method			Symm's Method	
N	E_M	E_A	N	E_M
16	2.8(−02)	3.8(−03)	64	2.52(−02)
32	3.2(−03)	7.0(−04)	128	3.90(−03)
64	8.4(−05)	2.7(−05)	256	6.00(−04)
128	1.2(−07)	1.8(−07)		

Example 5.3 *Frame of Limacon :*

Consider a pair of Limacon [9, p. 307]

$$\begin{aligned}\Gamma_0 : \{z(t) &= a_0 \cos t + b_0 \cos 2t + \mathrm{i}(a_0 \sin t + b_0 \sin 2t), a_0 > 0, b_0 > 0\},\\ \Gamma_1 : \{z(t) &= a_1 \cos t + b_1 \cos 2t + \mathrm{i}(a_1 \sin t + b_1 \sin 2t), a_1 > 0, b_1 > 0\},\end{aligned}$$

where $t : 0 \le t \le 2\pi$. When $b_1/b_0 = (a_1/a_0)^2$, the exact map is given by

$$f(z) = \frac{\sqrt{a_0^2 + 4b_0 z} - a_0}{2b_0},$$

which maps Γ_0 onto the unit circle and maps Γ_1 onto a circle of radius $\mu_1 = a_1/a_0$. Figure 5 shows the region and image based on our method. Table 9, 10, 11 and 12 show our results together with the results of Murid and Mohamed [11], Mohamed [10] and Symm [18].

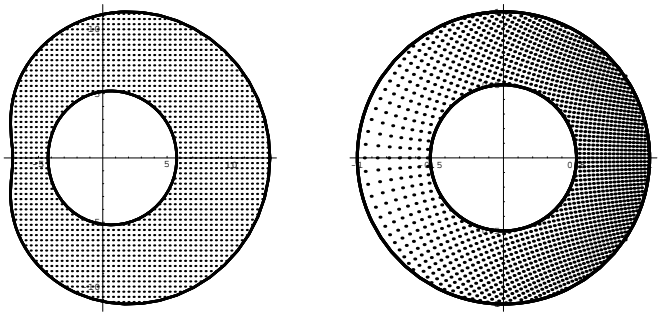

Figure 5: Frame of Limacons : a rectangular grid in Ω with grid size 0.4 and its image with $a_0 = 10, a_1 = 5, b_0 = 3$ and $b_1 = b_0/4$.

Table 9: Error Norm (Frame of Limacon) using our method

N	$\|\theta_0(t) - \theta_{0n}(t)\|_\infty$	$\|\theta_1(t) - \theta_{1n}(t)\|_\infty$	$\|\mu_1 - \mu_{1n}\|_\infty$	$\|\mu_1 - \mu_{1n}^*\|_\infty$
8	7.4(−04)	4.8(−04)	4.1(−03)	1.7(−03)
16	4.2(−06)	1.5(−06)	1.5(−05)	4.1(−04)
32	7.3(−11)	2.5(−11)	2.4(−10)	1.0(−04)
64	8.9(−16)	8.9(−16)	0	2.6(−05)

Table 10: Error Norm (Frame of Limacon) as given in [10] based on the Neumann kernel

N	$\|\theta_0(t)-\theta_{0n}(t)\|_\infty$	$\|\theta_1(t)-\theta_{1n}(t)\|_\infty$	$\|\mu_1-\mu_{1n}\|_\infty$
16	1.0(−05)	6.9(−06)	1.5(−05)
32	2.2(−09)	2.8(−09)	4.7(−10)
64	7.0(−09)	5.3(−09)	5.7(−10)

Table 11: Error Norm (Frame of Limacon) as given in [10, 11] based on the Kerzman-Stein kernel

N	$\|\theta_0(t)-\theta_{0n}(t)\|_\infty$	$\|\theta_1(t)-\theta_{1n}(t)\|_\infty$	$\|\mu_1-\mu_{1n}\|_\infty$
16	9.7(−06)	5.1(−06)	2.8(−05)
32	4.2(−10)	3.1(−10)	2.1(−10)
64	1.3(−15)	1.8(−15)	1.1(−16)

Table 12: Error Norm (Frame of Limacon) using Symm's method

N	64	128	256
E_M	6.3(−03)	1.0(−03)	2.0(−04)

Example 5.4 *Circular Frame :*
Consider a pair of circles [16, A-21]

$$\begin{aligned}\Gamma_0 : \{z(t) &= e^{it}\},\\ \Gamma_1 : \{z(t) &= c+\rho e^{it}\}, \qquad t : 0 \le t \le 2\pi\end{aligned}$$

such that the domain bounded by Γ_0 and Γ_1 is the domain between a unit circle and a circle center at c with radius ρ. The exact mapping function is given by

$$f(z)=\frac{z-\lambda}{\lambda z-1}, \quad \text{with } \lambda=\frac{2c}{1+(c^2-\rho^2)+\sqrt{(1-(c-\rho)^2)(1-(c+\rho)^2)}},$$

which maps Γ_0 onto the unit circle and Γ_1 onto a circle of radius

$$\mu_1=\frac{2\rho}{1-(c^2-\rho^2)+\sqrt{(1-(c-\rho)^2)(1-(c+\rho)^2)}}.$$

Figure 6 shows the region and image based on our method. Table 13, 15 and 14 show our results together with the results of Murid and Mohamed [11] and Mohamed [10].

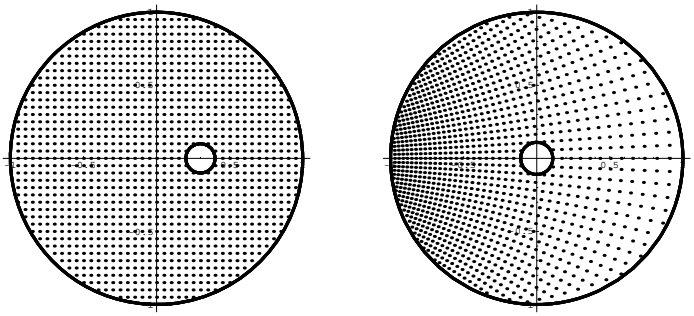

Figure 6: Circular Frame : a rectangular grid in Ω with grid size 0.05 and its image with $c = 0.3$ and $\rho = 0.1$.

Table 13: Error Norm (Circular Frame) using our method

N	$\|\theta_0(t) - \theta_{0n}(t)\|_\infty$	$\|\theta_1(t) - \theta_{1n}(t)\|_\infty$	$\|\mu_1 - \mu_{1n}\|_\infty$	$\|\mu_1 - \mu^*_{1n}\|_\infty$
4	5.1(−02)	1.1(−01)	2.6(−03)	1.6(−02)
8	8.7(−04)	1.7(−04)	3.7(−05)	3.7(−03)
16	1.3(−07)	2.5(−08)	4.7(−09)	8.8(−04)
32	1.3(−15)	8.9(−16)	4.2(−17)	2.2(−04)

Table 14: Error Norm (Circular Frame) as given in Mohamed [10] based on the Neumann kernel

N	$\|\theta_0(t) - \theta_{0n}(t)\|_\infty$	$\|\theta_1(t) - \theta_{1n}(t)\|_\infty$	$\|\mu_1 - \mu_{1n}\|_\infty$
8	3.6(−04)	6.9(−06)	5.1(−06)
16	3.7(−08)	7.2(−10)	6.2(−10)

Table 15: Error Norm (Circular Frame) as given in [10, 11] based on the Kerzman-Stein kernel

N	$\|\theta_0(t) - \theta_{0n}(t)\|_\infty$	$\|\theta_1(t) - \theta_{1n}(t)\|_\infty$	$\|\mu_1 - \mu_{1n}\|_\infty$
8	9.8(−11)	4.6(−09)	1.4(−06)
16	8.9(−16)	7.1(−15)	9.5(−11)

5.2 Triply Connected Regions

For our numerical examples involving triply connected regions, we have used two test regions, namely the regions bounded by an ellipse and two circles, and a region bounded by two ellipses and a circle. N number of collocation points on each boundary has been chosen. Since the exact mapping functions for the regions are unknown, we have compared our nemerical results with those obtained in [5, 8, 15].

Example 5.5 *Ellipse/two circles :*
Let

$$\begin{aligned}
\Gamma_0 : \{z(t) &= 2\cos t + \mathrm{i}\sin t\},\\
\Gamma_1 : \{z(t) &= 0.5\,(\cos t + \mathrm{i}\sin t)\},\\
\Gamma_2 : \{z(t) &= 1.2 + 0.3\,(\cos t + \mathrm{i}\sin t)\}, \quad t : 0 \le t \le 2\pi.
\end{aligned}$$

We have adopted the example problems from Reichel [15] and Kokkinos *et al.* [8] for comparison of μ_1, μ_2 and the angle of the slit, α (see Table 16). We obtain the results $\mu_1 = 0.42588654195460685$, $\mu_2 = 0.810970795718853$ and $\alpha = 0.715608$. Since the conditions of the problems are somewhat different, $\mu_0 = 1$ in ours and $\mu_0 = 1.5$ in Reichel's or $\mu_0 = 2$ in Kokkinos *et al.*, our radii μ_1 and μ_2 should be multiplied by 1.5 and 2 respectively. Values of μ_1 and μ_2 in Reichel [15] are denoted here by $\mu_{1,R}$ and $\mu_{2,R}$ respectively. While the values of μ_1, μ_2 and α in Kokkinos *et al.* [8] are denoted here by $\mu_{1,K}$, $\mu_{2,K}$ and α_K respectively. Figure 7 shows the region and its image based on our method.

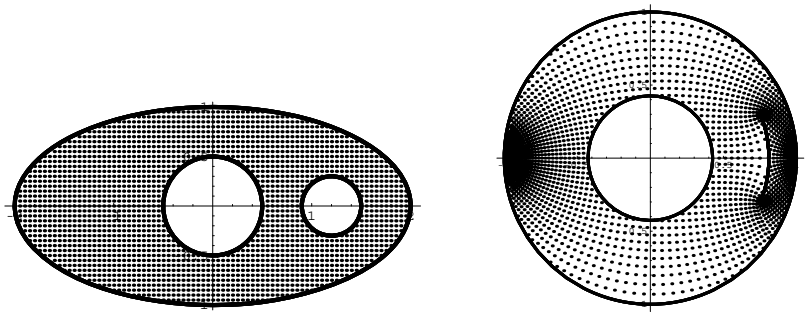

Figure 7: Ellipse/two circles : a rectangular grid in Ω with grid size 0.05 and its image.

Table 16: Radii comparison for Example 5.5 with [8, 15]

Reichel [15]		
N	$\|\mu_1 \times 1.5 - \mu_{1,R}\|_\infty$	$\|\mu_2 \times 1.5 - \mu_{2,R}\|_\infty$
16	1.4(−03)	1.3(−02)
32	9.8(−07)	6.6(−06)
64	8.6(−09)	4.9(−09)

Kokkinos *et al.* [8]			
N	$\|\mu_1 \times 2 - \mu_{1,K}\|_\infty$	$\|\mu_2 \times 2 - \mu_{2,K}\|_\infty$	$\|\alpha - \alpha_K\|_\infty$
16	1.4(−03)	1.3(−02)	8.7(−01)
32	9.7(−07)	6.6(−06)	1.3(−03)
64	2.0(−09)	7.1(−10)	2.8(−05)

Example 5.6 *Ellipse/Circle/Ellipse :*
Let

$$\begin{aligned}
\Gamma_0 : \{z(t) &= 2\cos t + \mathrm{i}\sin t\},\\
\Gamma_1 : \{z(t) &= 0.25\,(\cos t + \mathrm{i}\sin t)\},\\
\Gamma_2 : \{z(t) &= 1 + 0.5\cos t + 0.25\mathrm{i}\sin t\}, \quad t : 0 \le t \le 2\pi.
\end{aligned}$$

We have adopted the example problem from Ellacott [5] for comparison. Values of μ_1 and μ_2 in Ellacott [5] are denoted here by $\mu_{1,E}$ and $\mu_{2,E}$ respectively. See Table 17 for radii comparisons. Figure 8 shows the region and its image based on our method.

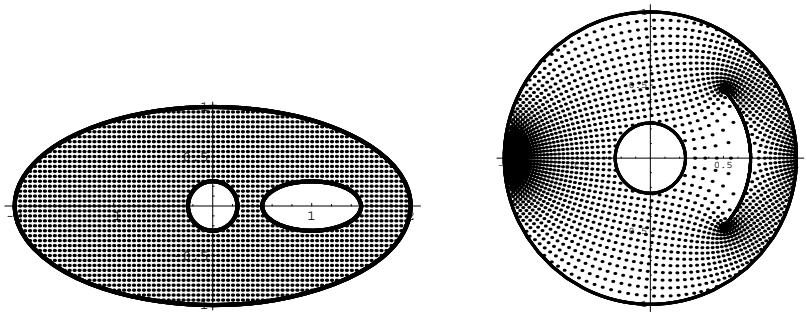

Figure 8: Ellipse/circle/ellipse : a rectangular grid in Ω with grid size 0.05 and its image.

Table 17: Radii comparison for Example 5.6 with [5]

N	Our Method	Ellacott [5]	Radii Comparison
64	$\mu_1 = 0.2406123854673435$	$\mu_{1,E} = 0.25$	$9.4(-03)$
	$\mu_2 = 0.6859816257842841$	$\mu_{2,E} = 0.68$	$6.0(-03)$

6 Conclusion

In this paper, we have constructed a new boundary integral equation for conformal mapping of regions of connectivity $M+1$ onto an annulus $\mu_1 < |w| < 1$ with circular slits of radii $\mu_2, ..., \mu_M$. The boundary integral equation involves the Neumann kernel and the unknown radii $\mu_1, ..., \mu_M$. Due to the presence of the unknown radii and together with some normalizing conditions, the discretized integral equation leads to a system of nonlinear algebraic equations which are solved using optimization method. Several mappings of the test regions were computed numerically using the proposed method. The advantage of our method is that it calculates the boundary correspondence functions and the unknown radii simultaneously with the same degree of accuracy. Having computed the boundary values of the mapping function, the interior values are then calculated by means of the Cauchy integral formula. The numercial examples show the effectiveness of the proposed method.

ACKNOWLEDGEMENTS. This work was supported in part by the Malaysian Ministry of Higher Education (MOHE) through the Research Management Centre (RMC), Universiti Teknologi Malaysia (FRGS Vote 78089). This support is gratefully acknowledged. The authors also wish to thank Professor Mohd Nor Mohamad of Department of Mathematics, Faculty of Science, Universiti Teknologi Malaysia for fruitful discussions.

References

[1] K. Amano, A Charge Simulation Method for the Numerical conformal mapping of interior, exterior and doubly connected domains, *J. Comp. Appl. Math.*, **53** (1994), 353–370.

[2] K. E. Atkinson, *A Survey of Numerical Methods for the Solution of Fredholm Integral Equations,* Society for Industry and Applied Mathematics, Philadephia, 1976.

[3] D. Crowdy, and J. Marshall, Conformal mapping between Canonical Multiply Connected Domains. *Computational Methods and Function Theory*, **6** (2006), 59-76.

[4] P. J. Davis, and P. Rabinowitz, *Methods of numerical integration, 2nd Edition,* Academic Press, Orlando, 1984.

[5] S. W. Ellacott, On the approximate conformal mapping of multiply connected domains, *Numerische Mathematik,* **33** (1979), 437–446.

[6] P. Henrici, *Applied and Computational Complex Analysis, Vol. 3,* John Wiley, New York, 1974.

[7] E. Hille, *Analytic Function Theory, Vol. 1,* Chelsea, New York, 1973.

[8] C. A. Kokkinos, N. Papamichael, and A. B. Sideridis, An orthonormalization method for the approximate conformal mapping of multiply-connected domains, *IMA Journal of Numerical Analysis,* **9** (1990), 343–359.

[9] P. K. Kythe, *Computational Conformal Mapping,* Birkhauser Boston, New Orleans, 1998.

[10] N. A. Mohamed, *An integral equation method for conformal mapping of doubly connected regions via the Kerzman-Stein and the Neumann kernels.* Master Thesis, Department of Mathematics, Universiti Teknologi Malaysia, 2007.

[11] A. H. M. Murid and N. A. Mohamed, An integral equation method for conformal mapping of doubly connected regions via the Kerzman-Stein kernel. *IJPAM,* **38**, No. 3(2007), 229–250.

[12] A. H. M. Murid and M. R. M. Razali, An integral equation method for conformal mapping of doubly-connected regions, *Matematika,* **15** (2)(1999), 79–93.

[13] Z. Nehari, *Conformal Mapping,* Dover Publications, Inc, New York, 1952.

[14] D. Okano, H. Ogata, K. Amano and M. Sugihara, Numerical conformal mapping of bounded multiply connected domains by the charge simulation method, *Journal of Comp. Appl. Math.,* **159** (2003), 109–117.

[15] L. Reichel, A fast method for solving certain integral equation of the first kind with application to conformal mapping, *Journal of Comp. Appl. Math.,* **14** (1986), 125–142.

[16] E. B. Saff and A. D. Snider, *Fundamentals of Complex Analysis,* Pearson Education, Inc, New Jersey, 2003.

[17] P. N. Swarztrauber, On the numerical solution of the dirichlett problem for a region of general shape, *SIAM J. Numer. Anal.,* **9**(2) (1972), 300–306.

[18] G. T. Symm, Conformal mapping of doubly connected domain, *Numer. Math.,* **13** (1969), 448–457.

[19] M. A. Wolfe, *Numerical Methods for Unconstrained Optimization,* Van Nostrand Reinhold Company, New Delhi, 1978.

[20] S. Wolfram, *Mathematica : A System of Doing Mathematics by Computer,* Redwood City, Addison-Wesley, 1991.

[21] C. Woodford, *Solving Linear and Non-Linear Equations,* McGraw-Hill, New York, 1992.

Received: September, 2008